Journal of Nuclear Materials 456 (2015) 461–466

Contents lists available at ScienceDirect

Journal of Nuclear Materials

journal homepage: www.elsevier.com/locate/jnucmat

The influence of glass composition on crystalline phase stability in glass-ceramic wasteforms

Ewan Maddrell [a,*], Stephanie Thornber [b], Neil C. Hyatt [b]

[a] National Nuclear Laboratory, Sellafield, Seascale, Cumbria CA20 1PG, UK
[b] Department of Materials Science and Engineering, The University of Sheffield, Mappin Street, Sheffield S1 3JD, UK

HIGHLIGHTS

- Crystalline phase formation shown to depend on glass matrix composition.
- Zirconolite forms as the sole crystalline phase only for most aluminous glasses.
- Thermodynamics indicate that low silica activity glasses stabilise zirconolite.

ARTICLE INFO

Article history:
Received 15 August 2014
Accepted 6 October 2014
Available online 14 October 2014

ABSTRACT

Zirconolite glass-ceramic wasteforms were prepared using a suite of Na_2O–Al_2O_3–B_2O_3–SiO_2 glass matrices with variable Al:B ratios. Zirconolite was the dominant crystalline phase only for the most alumina rich glass compositions. As the Al:B ratio decreased zirconolite was replaced by sphene, zircon and rutile. Thermodynamic data were used to calculate a silica activity in the glass melt below which zirconolite is the favoured crystalline phase. The concept of the crystalline reference state of glass melts is then utilised to provide a physical basis for why silica activity varies with the Al:B ratio.

1. Introduction

Glass-ceramic wasteforms are being developed for the immobilisation of a diverse range of plutonium containing residues on the Sellafield site [1,2]. The target crystalline phase is zirconolite ($CaZrTi_2O_7$), which acts as the host for plutonium, whilst the glass matrix is intended to digest the remainder of the residue. The wasteforms are to be produced by size reduction of the residue streams, blending with an appropriate precursor and consolidation by hot isostatic pressing (HIP). It is emphasised that the term glass-ceramic as used here differs from the established Materials Science concept of a glass-ceramic in that the zirconolite phase forms at the maximum HIP temperature, rather than by separate nucleation and growth heat treatments of a glass.

The current glass-ceramic precursor composition for immobilisation of the residues was derived empirically and is given in Table 1, and a typical glass-ceramic wasteform microstructure is shown in Fig. 1. The formulation in Table 1 arose because early inventories for the residues that would require immobilisation included a large quantity of calcium fluoride slags resulting from production of plutonium metal. To achieve the desired high waste loadings of this slag would lead to a low durability glass matrix with conventional glass formulations, so high alumina contents were used to improve the glass matrix leach resistance. Subsequently, the slags were removed from the residues inventory, greatly lowering the fluoride content of the glass matrix, but the high alumina level was retained. Consequently, calcium fluoride was required in the precursor to facilitate digestion of the residues and enhance growth of the zirconolite grains.

During process development work, a 100 kg batch of this precursor was prepared. An error in the batching was made such that the quantities of alumina and titania were interchanged. When this composition of precursor was HIPped, characterisation studies revealed that zirconolite had been destabilised, despite the fact that none of the zirconolite forming oxides had been reduced; this indicated that the glass composition plays an important role in determining the crystalline phase assemblage. Our initial hypothesis was that the lower alumina content of the misformulated precursor allowed the calcium oxide that is required to form zirconolite to remain dissolved in the glass.

The formulation in Table 1 was derived by an empirical approach and led to a non-classical glass matrix. Carter et al. [3] and Zhang et al. [4] took a more systematic approach to such glass-ceramic wasteforms. These wasteforms were targeted at

* Corresponding author. Tel.: +44 (0)1946 788903.
E-mail address: ewan.r.maddrell@nnl.co.uk (E. Maddrell).

http://dx.doi.org/10.1016/j.jnucmat.2014.10.010
0022-3115/

Hanford K-basin sludges and the immobilisation of the primary waste stream from production of molybdenum-99 at the Australian Nuclear Science and Technology Organisation site in Sydney respectively. In the work of Carter et al. and Zhang et al. the intended crystalline phase was the closely related titanate pyrochlore, $CaUTi_2O_7$. The glass matrix was formulated such that the trivalent species in the glass network, boron and aluminium, were charge compensated on a molar basis by sodium. The stoichiometric composition of the glass in this wasteform was $Na_2AlBSi_6O_{16}$. This glass provides a method by which the glass composition can be varied systematically. Given that the initial observations inferred an important role played by alumina, it was decided to prepare a suite of zirconolite glass-ceramics in which the glass matrix was defined by $Na_2Al_{1+x}B_{1-x}Si_6O_{16}$ to investigate the role played by glass composition in controlling crystalline phase stability. The $x = 1$ end member gives the mineral albite, $NaAlSi_3O_8$. The melting point of albite is 1120 °C [5] and the composition cools to a glass at the cooling rates that occur during a HIP cycle. From the available phase diagrams, [6] no boron analogue for albite was shown, and the liquidus estimated from the relevant phase diagram is 1100–1200 °C. No phase diagrams for the quaternary system Na_2O–Al_2O_3–B_2O_3–SiO_2 could be found.

Table 1
Composition of baseline glass-ceramic precursor.

Component	Wt.%
SiO_2	26.9
Al_2O_3	24.3
B_2O_3	5.3
Na_2O	6.1
CaO	6.6
Gd_2O_3	4.9
TiO_2	10.0
ZrO_2	10.9
CaF_2	5.0

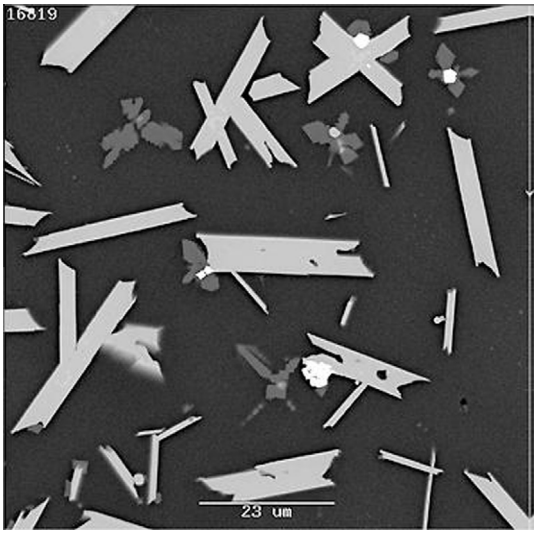

Fig. 1. Microstructure of baseline glass-ceramic wasteform. Light grey laths are zirconolite; mid grey dendrites are CaF_2; dark matrix is glass; bright inclusions are undigested actinide oxide.

2. Experimental

A suite of six samples was prepared based on the glass composition $Na_2Al_{1+x}B_{1-x}Si_6O_{16}$ described above, with $x = 0$–1 in increments of 0.2. The standard batch size comprised nominally 50 g of glass together with 0.25 moles of the zirconolite forming oxides. This blend gives an approximately equivolume mixture of glass and crystalline material if zirconolite forms as the crystalline phase.

The glass forming components were supplied by silica, alumina, sodium metasilicate and the glass frit used for high level waste vitrification on the Sellafield site. The latter component was chosen as a stable source of boron oxide. The glass frit is a mixed alkali borosilicate glass containing both sodium and lithium and for the purposes of glass composition calculation lithium was treated as being a molar equivalent for sodium. In all formulations, sodium accounted for at least 85 mol% of the total alkali. The crystalline phase forming oxides were added as perovskite ($CaTiO_3$), titania and zirconia. The compositions of the six glass-ceramic samples are summarised by mass in Table 2, and the glass compositions are presented by mole in Table 3; the absolute molar quantities are then normalised to indicate the composition according to the overarching formula – $Na_2Al_{1+x}B_{1-x}Si_6O_{16}$. Note that because the glass components were calculated to give a constant nominal mass per batch, the molar amount of glass decreases slightly as alumina is substituted in for boron oxide in the glass network.

All samples were prepared from standard laboratory reagents. Powder batches were milled in a Retsch PM 100 planetary mill for 20 min at 300 rpm using a 250 ml hardened steel pot and 10 mm diameter balls. 2-Propanol was used as a carrier fluid and the slurry dried at 80 °C. The dried powders were packed into straight-walled stainless steel HIP cans using a uniaxial pressure of 50 MPa. After welding on the lids, which included evacuation tubes, the HIP cans were baked out and evacuated at 600 °C for a minimum of 4 h and sealed. The samples were then HIPped at 1250 °C and 100 MPa with a 2 h dwell. Heating rates were 10 °C min^{-1}–900 °C,

Table 2
Composition of model glass-ceramics (g).

	$x = 0$	$x = 0.2$	$x = 0.4$	$x = 0.6$	$x = 0.8$	$x = 1.0$
HIP can	NS274	NS275	NS276	NS277	NS278	NS279
Glass frit	15.22	12.10	9.02	5.98	2.97	0.00
Na_2SiO_3	6.90	7.87	8.83	9.78	10.71	11.64
SiO_2	22.41	23.69	24.95	26.20	27.43	28.64
Al_2O_3	5.01	5.98	6.93	7.87	8.80	9.72
$CaTiO_3$	33.99	33.99	33.99	33.99	33.99	33.99
ZrO_2	30.81	30.81	30.81	30.81	30.81	30.81
TiO_2	19.97	19.97	19.97	19.97	19.97	19.97

Table 3
Composition of glass matrices on a molar basis.

	NS274		NS275		NS276		NS277		NS278		NS279	
	Moles	Norm'd	Moles	Norm'd	Moles	Norm'd	Moles	Norm'd	Moles	Norm'd	Moles	Norm'd
SiO_2	0.5902	6.000	0.5865	6.000	0.5828	6.000	0.5792	6.000	0.5756	6.000	0.5720	6.000
$NaO_{0.5}$	0.1688	1.716	0.1733	1.773	0.1777	1.830	0.1821	1.886	0.1864	1.943	0.1907	2.000
$LiO_{0.5}$	0.0279	0.284	0.0222	0.227	0.0165	0.170	0.0110	0.114	0.0054	0.057	0	0.000
$BO_{1.5}$	0.0984	1.000	0.0782	0.800	0.0583	0.600	0.0386	0.400	0.0192	0.200	0	0.000
$AlO_{1.5}$	0.0984	1.000	0.1173	1.200	0.1360	1.400	0.1544	1.600	0.1727	1.800	0.1907	2.000
Sum	0.9837	10	0.9775	10	0.9713	10	0.9653	10	0.9593	10	0.9534	10

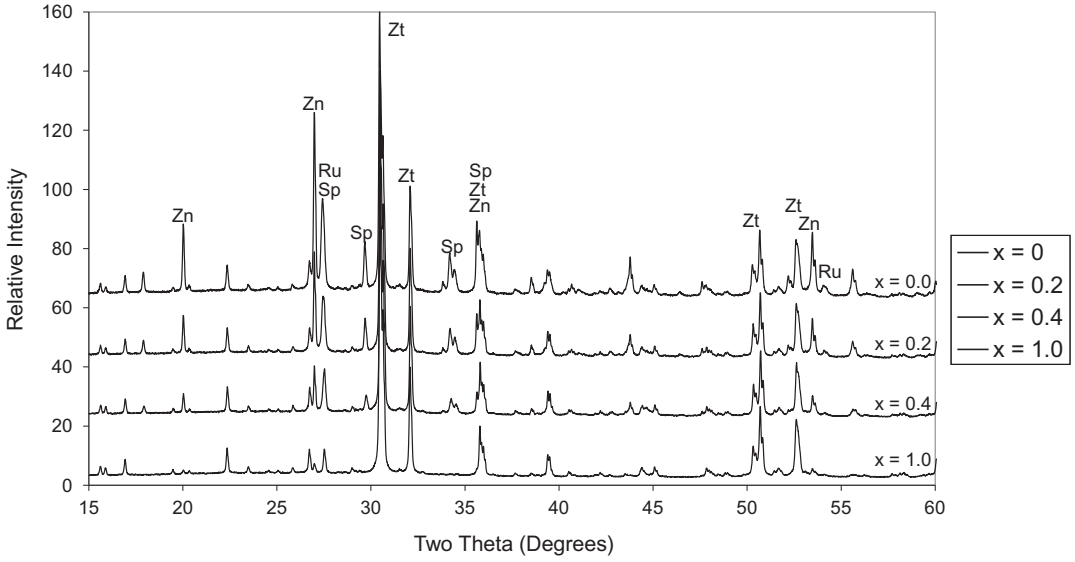

Fig. 2. XRD trace from $x = 0$, 0.2, 0.4 and 1.0 sample. The main diagnostic peaks for each phase are indicated: zirconolite (Zt); zircon (Zn); sphene (Sp) and rutile (Ru).

8 °C min^{-1}–1000 °C, 6 °C min^{-1}–1100 °C, 4 °C min^{-1}–1200 °C and 2 °C min^{-1}–1250 °C; cooling was at 10 °C min^{-1} until reduced by insufficient thermal transfer away from the HIP hot zone.

After HIPping the samples were removed from the HIP cans and analysed by X-ray diffraction (XRD) [Bruker D2 Phaser operating with Ni filtered Cu Kα radiation and a position sensitive detector] and scanning electron microscopy (SEM) operating in the backscattered electron mode and energy dispersive spectroscopy (EDS) [Jeol JSM 5600 and PGT IMIX].

3. Results and discussion

3.1. X-Ray diffraction

XRD patterns from the $x = 0$, 0.2, 0.4 and 1.0 samples are shown in Fig. 2 – the most intense reflections for each phase are annotated. Although the intended zirconolite phase is apparent in all four traces it is clear that other crystalline phases have also formed, and that their abundance, inferred by the relative intensity of peaks, decreases as the Al:B ratio increases. In conjunction with SEM/EDS the secondary phases were identified as zircon, ($ZrSiO_4$) sphene ($CaTiSiO_5$) and rutile (TiO_2). Rutile is somewhat difficult to identify unambiguously by XRD because of peak overlaps, and the strongest reflection that is unique to rutile is that at $2\theta = 54°$. In the $x = 1.0$ composition, that is the aluminous end member of the suite of samples, the most intense reflection from the secondary phases, the {200} of zircon at $2\theta = 27°$, shows that zircon is present only as a trace; and there is no evidence from XRD for sphene and rutile. The XRD data are presented with comprehensive indexing as Fig. A1 in the Appendix.

3.2. Scanning electron microscopy

The microstructure of the $x = 0$ sample is shown in Fig. 3. On first inspection the atomic number contrast suggested two crystalline phases exist, which appear with light grey and mid grey contrast against the dark glass matrix. Closer examination revealed slight brightness differences in both contrast levels. EDS analysis of the crystalline phases indicated that for the light grey phase, the brighter of the two contrast levels corresponded to zircon whereas the darker was zirconolite. Of the two mid grey phases, the brighter was rutile and darker was sphene.

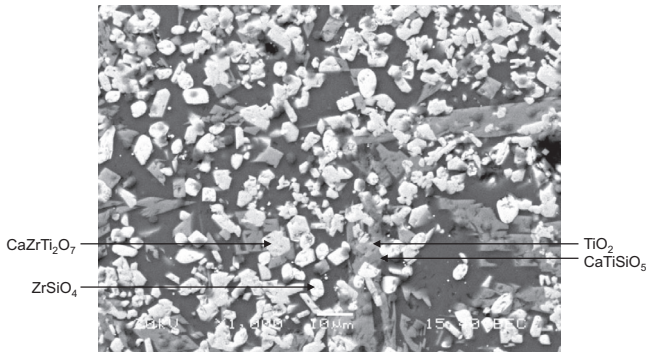

Fig. 3. Microstructure of $x = 0$ sample.

3.3. Thermodynamic perspective

It is clear that the experimental evidence did not support the initial hypothesis relating to increased solubility of calcium oxide in alumina poor glasses, because calcium oxide readily formed sphene rather than zirconolite in these compositions. As the alumina content of the glass matrix increased with x, the amount of sphene, zircon and rutile decreased until at $x = 0.8$ and $x = 1.0$ zircon was present only as a trace, and sphene and rutile were absent based on XRD traces. Hence, based on the observed phases it is suggested that there is an equilibrium:

$$CaZrTi_2O_7 + 2[SiO_2] \rightleftharpoons CaTiSiO_5 + ZrSiO_4 + TiO_2 \quad (1)$$

where $[SiO_2]$ represents silica as a component of a glass melt.

The competing reactions can be compared thermodynamically by:

$$CaO + ZrO_2 + 2TiO_2 + 2SiO_2 \rightarrow CaZrTi_2O_7 + 2SiO_2$$

and

$$CaO + ZrO_2 + 2TiO_2 + 2SiO_2 \rightarrow CaTiSiO_5 + ZrSiO_4 + TiO_2$$

The relevant standard Gibbs free energies of formation are:

$CaO = -603.1$ kJ mol^{-1} [7]
$ZrO_2 = -1042.9$ kJ mol^{-1} [7]
$TiO_2 = -888.8$ kJ mol^{-1} [7]
$SiO_2 = -856.3$ kJ mol^{-1} [7]
$CaZrTi_2O_7 = -3515.6$ kJ mol^{-1} [7]

$ZrSiO_4$ = −1919.7 kJ mol^{-1} [7]
$CaTiSiO_5$ = −2456.2 kJ mol^{-1} [8]

It is recognised that these data are for a temperature of 298.15 K, but in the absence of high temperature data it is necessary to make the assumption that they will remain essentially invariant with temperature. Inspection of a wider range of data for the formation of mixed oxides from their parent oxides indicates this approximation is reasonable [9].

From these data it can be calculated that the standard Gibbs free energy for the formation of zirconolite and silica from the relevant oxides is −92.0 kJ mol^{-1}; and for the formation of sphene, zircon and rutile it is −128.5 kJ mol^{-1}. The thermodynamic data therefore indicate that the equilibrium for the principal reaction (Eq. (1)), with all phases in the standard state, lies to the right; that is, zirconolite is *not* the thermodynamically favoured phase. The overall free energy benefit in favour of sphene and zircon is -36.5 kJ mol^{-1}. To verify this analysis, a fully crystalline sample was prepared by sintering the above mixture of oxides at 1300 °C for 50 h. XRD of this sample confirmed formation of a phase assemblage of sphene, zircon and rutile as shown by the diffraction pattern in Fig. 4. The XRD data are presented with comprehensive indexing as Fig. A2 in the Appendix.

Building on this perspective, qualitatively it can be observed that the equilibrium for the principal reaction (Eq. (1)) will move towards zirconolite at low silica activity. To quantify this the critical silica activity can be estimated as follows. For any equilibrium reaction:

$\Delta G = \Delta G^{\ominus} + RT \ln Q_r$

where Q_r is the reaction quotient defined here by:

$$Q_r = [CaTiSiO_5][ZrSiO_4][TiO_2]/[CaZrTi_2O_7][SiO_2]^2$$

where $[CaTiSiO_5]$ represents the chemical activity of sphene etc; and $\Delta G^{\ominus}$ is the standard free energy change associated with the forward reaction, calculated above as −36.5 kJ mol^{-1}.

At equilibrium $\Delta G = 0$ and the activity of all crystalline phases can be taken as unity. Hence the reaction quotient reduces to:

$$Q_r = [SiO_2]^{-2}$$

From this analysis the activity of silica in the glass matrix when the crystalline phase reaction is at equilibrium at 1250 °C can be calculated as 0.24. Current work is trying to put this thermodynamic perspective onto a firmer footing.

The findings here can be compared with other work on glass-ceramic nuclear wasteforms by Loiseau et al. [10–12]. The materials in these studies were prepared by the established glass-ceramic method of quenching followed by nucleation and growth heat treatments. Loiseau et al. showed that zirconolite was the crystal phase that formed in the bulk of a sample, presumably by homogeneous nucleation, whereas anorthite ($CaAl_2Si_2O_8$) and sphene, formed by heterogeneous nucleation, were observed in surface regions. Long term heat treatments of these samples indicated that zirconolite was gradually replaced by sphene, anorthite and free zirconia. This work again demonstrates the relative thermodynamic instability of zirconolite, although the heat treatments required for this phase to be destabilised could not credibly occur during long term wasteform storage and disposal.

3.4. General comments

This quantitative thermodynamic perspective does not necessarily lead to a physical understanding of why silica activity varies with glass composition, and with it crystalline phase formation; hence, our understanding of why zirconolite becomes the favoured phase in more alumina rich glass systems remains embryonic.

Initially, a simple mass balance was conducted in which it was assumed that the calcium oxide, zirconia and titania were partitioned exclusively into the four crystalline ceramic phases. The remainder, containing the alkali oxide, boron oxide, alumina and silica not incorporated in zircon or sphene, was available to form a glass. As the relative amount of the crystalline phases was varied, the quantity of silica in the remainder changed. For the higher alumina content samples, the remainder did not have a viable glass forming composition when too much of the silica was consumed by sphene and zircon. As silica was consumed, the composition of the remainder tended towards that of nepheline/carnegieite ($NaAlSiO_4$) which has a melting point of 1520 °C. Formation of zirconolite liberated silica and made the remainder more amenable to glass formation. It is possible that the thermodynamic benefit of forming a high entropy glass offsets the detriment of forming the less stable crystalline phase. When the remainder contained increased levels of boron oxide, as silica was removed from the target matrix composition the liquidus temperature decreased slightly and glass formation remained viable despite silica being partitioned into zircon and sphene. That said, the liquidus

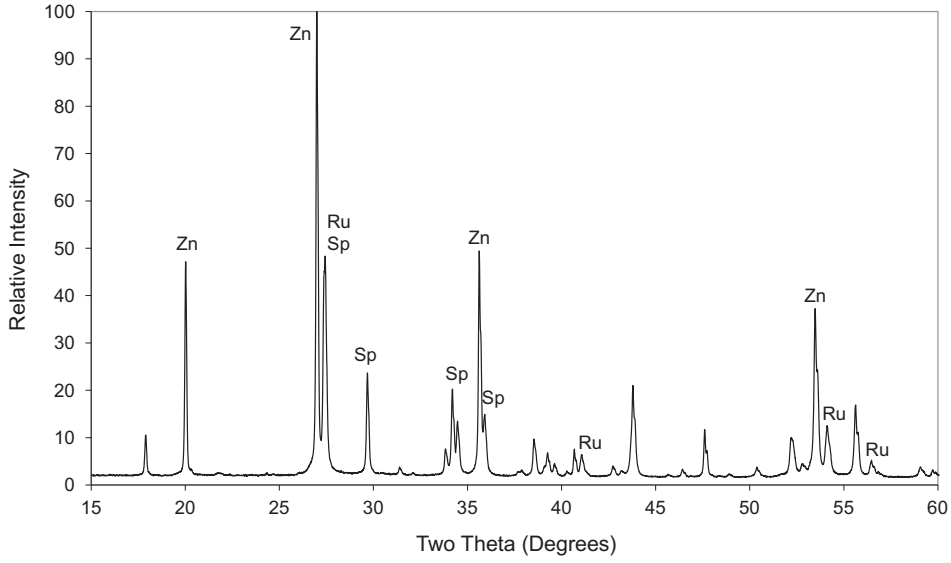

Fig. 4. XRD trace from fully crystalline sample. The main diagnostic peaks for each phase are indicated: zircon (Zn); sphene (Sp) and rutile (Ru).

temperature of the albite–nepheline tie shows a eutectic, [5] hence silica poor deviations from the albite composition will still be amenable to glass formation and this argument may not explain the near complete elimination of silicate phases from the most aluminous samples, as indicated by XRD. Indeed, the mass balance approach showed that a remainder corresponding to the eutectic composition formed when 30% of the calcium oxide, titania and zirconia existed as zircon, sphene and rutile.

An alternative approach is to consider the concept of the crystalline reference state (CRS) for glass melts, as discussed by Conradt [13]. The CRS for any multi-component glass is the set of equilibrium crystalline phases that will form if the melt is cooled sufficiently slowly for crystallisation to occur. Typically, even a simple three component melt will have a CRS defined by three phases, because the glass composition will rarely correspond to an exact crystalline phase. In the $Na_2Al_{1+x}B_{1-x}Si_6O_{16}$ system under study, for the aluminous glass end member the CRS is clearly albite. Notwithstanding the evidence from phase diagrams, a boron analogue of albite is known, the mineral reedmergnerite, but the syntheses described by Fleet [14] suggest it does not crystallise readily from the melt. The phase is not recorded in the most recent Na_2O–B_2O_3–SiO_2 phase diagram that we can find [6]. Note that no quaternary Na_2O–Al_2O_3–B_2O_3–SiO_2 phases are documented, so the CRS of four component glasses is defined by the Na_2O–B_2O_3–SiO_2 and Na_2O–Al_2O_3–SiO_2 systems. To quote from Conradt,

> *"Indeed, there is ample experimental evidence that the heterogeneous nature of the CRS is reflected by the properties of a glass and its melt. ..... Likewise, structural investigations reveal that the number and kind of structural (Short Range Order) entities in oxide glasses follow quite stringent rules of coexistence. In the cited cases, the species can be unambiguously related one by one to the constitutional compounds of the CRS – not necessarily with respect to their actual structure, but to their number and stoichiometry."*

Consequently, if the tendency for reedmergnerite to form is weak, it may be absent from the *de facto* CRS for the boron end member, and the CRS now includes silica along with the boron analogue of nepheline ($NaBSiO_4$) or even $NaBO_2$ – the available phase diagram is equivocal over the stability of the former compound. If silica is a component of the *de facto* CRS for the boron end member, this may provide a physical basis for the thermodynamic argument that the activity of silica is higher in more boron rich glasses.

4. Conclusions

The formation of crystalline phases in glass-ceramic wasteforms has been shown to be dependent on the composition of the glass matrix. Based on available thermodynamic data for the free energy of formation of the relevant crystalline phases, it is argued that zirconolite becomes the preferred crystalline phase at low silica activities – below $[SiO_2] = 0.24$ at 1250 °C. This criterion is apparently satisfied in the more aluminous glass compositions studied. The concept of the crystalline reference state of a glass melt has been briefly discussed to provide a physical understanding of why this occurs.

Acknowledgments

The support of Sellafield Limited is acknowledged for fabrication of the initial samples. This research was part supported by EPSRC under grant EP/L014041/1, and by provision of a studentship to ST with support from the Nuclear Decommissioning Authority. NCH is grateful to the Royal Academy of Engineering and Nuclear Decommissioning Authority for funding.

Appendix

The appended Figs. A1 and A2 provide a detailed indexation of the XRD traces in Figs. 2 and 4 respectively. In Fig. A1 it can be seen that through the progression of glass formulation from samples 274 to 276 that the amounts of zircon, sphene and rutile decrease. And by sample 279, only a trace of zircon remains from these three phases. This trend is most clearly apparent when following the zircon peak at $2\theta = 27°$ and the sphene peak at $2\theta = 30°$. In Fig. A2, for the crystalline phase forming oxides sintered in the absence of a glass matrix, the most intense reflection from the zirconolite phase, at $2\theta = 30.5°$, is conspicuous by its absence.

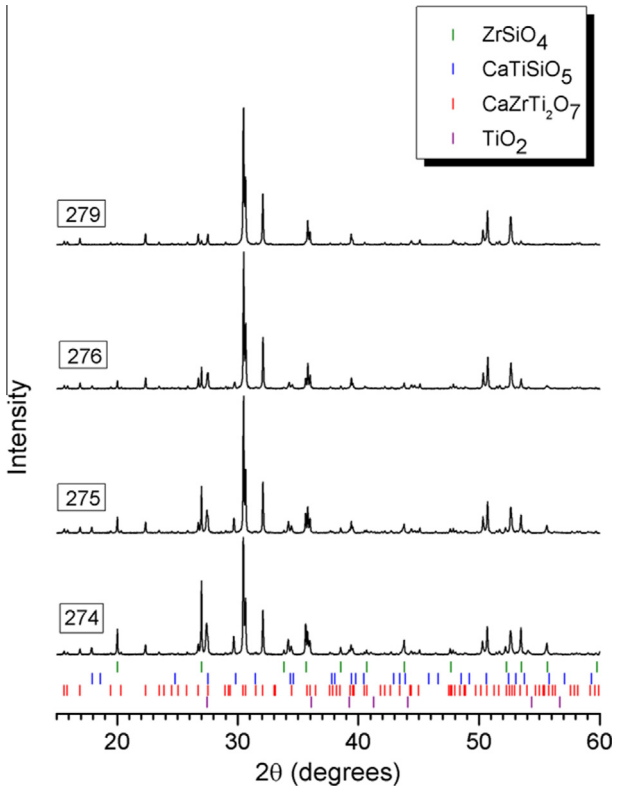

Fig. A1. XRD traces from $x = 0$, 0.2, 0.4 and 1.0 samples with comprehensive peak indexing.

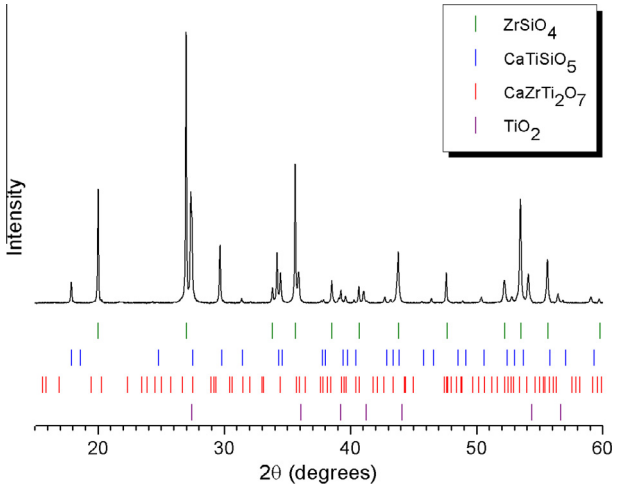

Fig. A2. XRD trace from fully crystalline sample with comprehensive peak indexing.

References

[1] C.R. Scales, E.R. Maddrell, N. Gawthorpe, B.D. Begg, S. Moricca, R.A. Day, M.W.A. Stewart. Demonstrating a glass-ceramic route for the immobilisation of plutonium containing wastes and residues on the Sellafield site. in: Proceedings WM'06, 2006.

[2] M. W. A. Stewart, S.A. Moricca, B.D. Begg, R.A. Day, C.R. Scales, E.R. Maddrell, A.B. Eilbeck, Flexible process options for the immobilisation of residues and wastes containing plutonium, in: The 11th International Conference on Environmental Remediation and Radioactive Waste Management, Am. Soc. Mech. Eng., 2007, pp. 1453–60.

[3] M.L. Carter, H. Li, Y. Zhang, A.L. Gillen, E.R. Vance, HIPped tailored pyrochlore-rich glass-ceramic waste forms for the immobilization of nuclear waste, in: Scientific Basis for Nuclear Waste Management XXXII Materials Research Society Proceedings, vol. 1124, Cambridge University Press, 2009.

[4] Y. Zhang, Z. Zhang, G. Thorogood, E.R. Vance, J. Nucl. Mater. 432 (1) (2013) 545–547.

[5] J.W. Greig, T.F.W. Barth, Fig. 507 in Phase Diagrams for Ceramists, Publ. Am. Ceram. Soc. 1964, 5th Ser., vol. 35A, Am. J. Sci., 1938, p. 94.

[6] G.W. Morey, Fig. 515 in Phase Diagrams for Ceramists, publ. Am. Ceram. Soc. 1964, vol. 35, J. Soc. Glass Tech., 1951, p. 270.

[7] R.L. Putnam, U.F. Gallegos, A. Navrotsky, K.B. Helean, S.V. Ushakov, B.F. Woodfield, J. Boerio-Goates, B.B. Ebbinghaus, M.A. Williamson, Formation energetics of ceramic phases related to surplus plutonium disposition, in: Environmental Issues and Waste Management Technologies VI, Ceramic Transactions 119, Publ. American Ceramic Society, 2001, pp. 147–58

[8] M.R.F. Manon, E. Dachs, E.J. Essene, Contrib. Mineral. Petrol. 156 (6) (2008) 709–720.

[9] Table 8.8i in Smithells Metals Reference Book, 7th ed., Publ. Butterworth Heinmann, 1992.

[10] P. Loiseau, D. Caurant, O. Majerus, N. Baffier, C. Fillet, J. Mater. Sci. 38 (4) (2003) 843–852.

[11] P. Loiseau, D. Caurant, O. Majerus, N. Baffier, C. Fillet, J. Mater. Sci. 38 (4) (2003) 843–852.

[12] P. Loiseau, D. Caurant, O. Majerus, N. Baffier, C. Fillet, Mater. Res. Soc. Proc. 807 (2004) 359–364.

[13] R. Conradt, J. Non-Cryst. Sol. 345–346 (2004) 16–23.

[14] M.E. Fleet, Am. Min. 77 (1992) 76–84.